CCFE
CULHAM CENTRE FOR FUSION ENERGY

UK Atomic Energy Authority

UKAEA-CCFE-CP(18)02

F.J. Casson, H. Patten, C. Bourdelle, S. Breton, J. Citrin, F. Koechl, C. Angioni, Y. Baranov, R. Bilato, E. Belli, C.D. Challis, G. Corrigan, A. Czarnecka, O. Ficker, L. Garzotti, M. Goniche, J.P. Graves, T. Johnson, K. Kirov et al

Predictive multi-channel flux-driven modelling to optimise ICRH tungsten control in JET

Predictive multi-channel flux-driven modelling to optimise ICRH tungsten control in JET

F.J. Casson, H. Patten, C. Bourdelle, S. Breton, J. Citrin, F. Koechl, C. Angioni, Y. Baranov, R. Bilato, E. Belli, C.D. Challis, G. Corrigan, A. Czarnecka, O. Ficker, L. Garzotti, M. Goniche, J.P. Graves, T. Johnson, K. Kirov et al

This paper has been submitted to
27th IAEA Fusion Energy Conference, Ahmedabad, India, 22-27 October 2018

PREDICTIVE MULTI-CHANNEL FLUX-DRIVEN MODELLING TO OPTIMISE ICRH TUNGSTEN CONTROL IN JET

F.J. Casson[1], H. Patten[2], C. Bourdelle[3], S. Breton[3], J. Citrin[4], F. Koechl[1], C. Angioni[5], Y. Baranov[1], R. Bilato[5], E.A. Belli[6], C.D. Challis[1], G. Corrigan[1], A. Czarnecka[7], O. Ficker[8], L. Garzotti[1], M. Goniche[3], J.P. Graves[2], T. Johnson[9], K. Kirov[1], P. Knight[1], E. Lerche[1,10], M. Mantsinen[11], J. Mylnar[8], M. Sertoli[5,1], M. Valisa[12], and JET contributors*

EUROfusion Consortium, JET, Culham Science Centre, Abingdon, UK
*[1]UKAEA, Abingdon, UK – [2]EPFL-SPC, Lausanne, Switzerland - [3]CEA, Saint-Paul-lez-Durance, France - [4]DIFFER, Eindhoven, The Netherlands – [5]IPP, Garching, Germany – [6]General Atomics, San Deigo, USA - [7]IPPLM, Warsaw, Poland – [8]IPP-CAS, Prague, Czech Republic – [9]KTH, Stockholm, Sweden - [10]LPP-ERM/KMS, Brussels, Belgium - [11]BSC-CNS, Barcelona, Spain – [12]RFX, Padova, Italy - *See the author list of X. Litaudon et al 2017 Nucl. Fusion 57 102001*

Abstract

The evolution of the JET high performance hybrid scenario, including central accumulation of the tungsten (W) impurity, is reproduced with predictive multi-channel integrated modelling over multiple confinement times using first-principle based models. 8 transport channels ($T_i, T_e, j, n_D, n_{Be}, n_{Ni}, n_W, \omega$) are modelled predictively, with self-consistent sources, radiation and magnetic equilibrium, yielding a system with multiple non-linearities which can produce a radiative temperature collapse after several confinement times. W is transported inward by neoclassical convection driven by the main ion density gradients and enhanced by poloidal asymmetries due to centrifugal acceleration. The slow evolution of the bulk density profile sets the timescale for W accumulation. Prediction of this phenomenon requires a turbulent transport model capable of accurately predicting particle and momentum transport (QuaLiKiz) and a neoclassical transport model including the effects of poloidal asymmetries (NEO) coupled to an integrated plasma simulator (JINTRAC). The modelling capability is applied to optimise the available actuators to prevent W accumulation, and to extrapolate in power and pulse length. Central NBI heating is preferred for high performance, but comes at the price of central deposition of particles and torque which pose the risk of W accumulation. The primary mechanisms for ICRH to control W in JET are via its impact on the bulk profiles and turbulent diffusion. High power ICRH near the axis can sensitively mitigate against W accumulation, and ion heating (He-3 minority) is predicted to provide more resilience to W accumulation than electron heating (H minority) in the JET hybrid. Extrapolation to DT plasmas finds 15MW of fusion power and improved confinement compared to DD, due to reduced ion-electron energy exchange, and increased Ti/Te stabilisation of ITG instabilities. The turbulence reduction in DT increases density peaking and accelerates the arrival of W on axis; this may be mitigated by reducing the penetration of the beam particle source with an increased pedestal density.

1. INTRODUCTION

The “hybrid” scenario is one of two high performance H-mode scenarios developed in JET with the ITER-like wall for a future DT campaign [1]; it operates at a lower density and higher β compared to the alternative high current “baseline” scenario. The goal for both DT scenarios is to produce 15MW of fusion power for 5s. To produce a steady high performance plasma, the hybrid scenario development must address three connected challenges: i) to maintain divertor heat loads within acceptable limits, ii) to control the accumulation of the radiative tungsten (W) impurity in the plasma core, and iii) to avoid performance limiting MHD modes.

In this work, we use the word “accumulation” to refer to the inward radial transport of impurities, which leads to their increasing concentration *near the magnetic axis*. The mechanism responsible for central W accumulation is inward neoclassical convection driven by main ion density gradients and strongly enhanced by poloidal asymmetries [2]. The slow timescale of main ion density evolution over multiple confinement times (Fig. 1) sets the timescale for central W accumulation [2,3]. Central NBI heating is the main actuator necessary for high performance in the hybrid scenario, but comes at the price of central deposition of particles and torque which pose the risk of W accumulation [3]. Central ICRH has multiple beneficial effects which can mitigate this, including: **1)** Flattening the bulk plasma density and rotation profile through an increase in turbulence relative to the NBI source, **2)** Increasing turbulent diffusion of the tungsten impurity, **3)** Increasing the neoclassical temperature screening from both main ions and fast ions, enhancing the outward neoclassical W convection [4], and **4)** Reduction of tungsten poloidal asymmetry through the parallel force balance with an anisotropic minority, reducing the neoclassical convection [4,5]. These various ICRH effects create a space for potential optimisation, which is a challenge for predictive modelling, requiring both integrated flux-driven simulations and high-fidelity ICRH modelling.

This work presents the validation of a recently developed multi-channel flux-driven predictive capability for all core transport channels using first-principle based models, which reproduces the evolution of the hybrid scenario over multiple confinement times, including the central W accumulation and associated radiative collapse. Building on a first presentation of this capability in [3] for NBI only plasmas, the accuracy of W accumulation predictions are here refined, and extended to cases including ICRH, supported by detailed ICRH modelling. The modelling tools are applied to understand and optimise the available actuators of plasma heating to prevent W accumulation, and to extrapolate to high power, longer pulses and to the planned DT campaign on JET.

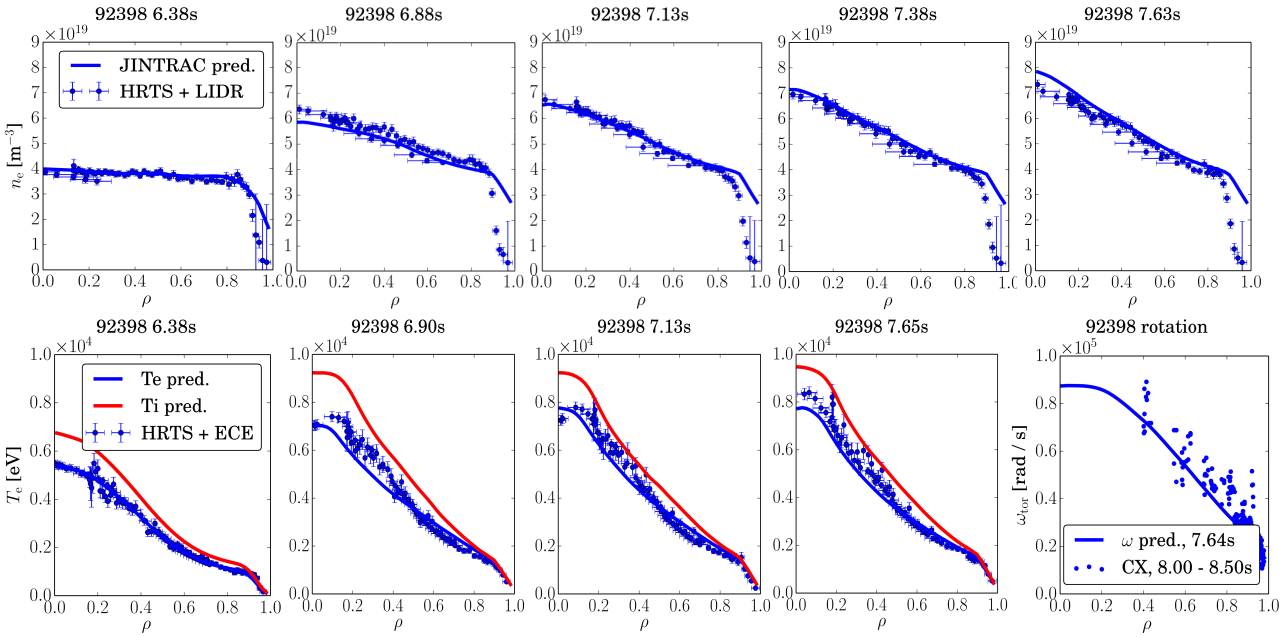

FIG. 1. Evolution of predicted bulk plasma profiles in multi-channel JINTRAC-QuaLiKiz-NEO simulation compared to experimental measurements for JET 92398. The simulation is initialised at 6.38s with profiles fitted from measurements just after the H mode and full NBI power are established. After the initial condition, the core plasma is simulated fully self-consistently without using any experimental input data. Boundary conditions at the LCFS are constant in time, and pedestal top target values, matched to experiment, are constant after 6.9s. Core Ti measurements are unavailable; neutron rate analysis supports Ti~1.25Te.

2. MODELS AND ASSUMPTIONS

An accurate predictive description of W accumulation requires a turbulent transport model capable of correctly predicting particle and momentum transport channels (in addition to the energy channels), and a neoclassical transport model which includes poloidal asymmetries due to the centrifugal force and fast ion anisotropies. For this work, these requirements have been met by coupling the drift kinetic neoclassical solver NEO [6] and the fast quasilinear gyrokinetic model QuaLiKiz [7,8] to the integrated modelling suite JINTRAC [9,10], allowing 8 transport channels $T_i, T_e, j, n_D, n_{Be}, n_{Ni}, n_W, \omega$, magnetic equilibrium, sources and radiation to all be evolved self-consistently. In all cases presented, the QuaLiKiz transport model is run with the inclusion of ExB shear from mid-radius outwards, and with ITG, TEM and ETG scales included (indicated as most appropriate from previous validation studies [8, 11]), but without poloidal asymmetries. An ad-hoc model is added to mimic the effect of electromagnetic stabilisation of the ITG instability, known to be significant in JET hybrid [12]: the ∇T_i inputs to QuaLiKiz are reduced by a factor of the local $\beta_{thermal}/\beta_{total}$, (between 0.7 and 1 in the reference discharge) shifting the ITG threshold and correcting the under-prediction of Ti otherwise observed in QuaLiKiz simulations of hybrid discharges [3,8] (the factor used emphasises fast ion EM effects, cross-correlated *in JET* with total β). In all cases presented, NEO is run including the effect of poloidal asymmetries (which increase neoclassical W transport 20x in strongly rotating JET plasmas).

NBI heating is simulated self-consistently with the PENCIL code [13]. For the reference discharge, the H minority ICRH is also simulated self-consistently with PION [14], but in the later sensitivity and extrapolation studies, prescribed ICRH profiles are used (and compared with advanced models). The ICRH minority is not included in the transport equations. The fixed boundary equilibrium is solved with ESCO. The plasma is modelled from the last closed flux surface to the axis, using a fixed pedestal width with a continuous (averaged) ELM model which adjusts anomalous pedestal transport in feedback control to a specified height. The boundary conditions at the LCFS (from data) are Ti=Te=120eV, n_D = 2.2e19 m^{-3}, V_{tor} = 47 km/s (LFS). The pedestal top density and temperature targets are taken from fits to experimental data, ramped gradually during the first 0.5s following the experimental evolution, and constant thereafter (Te = 1500eV, Ti = 1650eV, ne = 3.9e19 m^{-3}). The anomalous pedestal momentum transport is inferred from the ion transport with Prandtl no. = 0.9. The SOL neutral source is modelled with the cold neutral model FRANTIC [15], also in feedback control, with a time-averaged particle source representing a ~10% fuelling efficiency from the gas puff. All charge states of the impurities Be, Ni and W are evolved, but only the average local charge is used to evaluate transport for each impurity. ADAS data are used for ionisation, recombination and radiation. For W, an improved ADAS radiation model [16] is used. No core MHD models are used. Inside the pedestal top, the predictions depend only on first-principle based models without adjustment of free parameters, with limited exceptions: 1) A minimum level of background transport is set at 3% of the standard Bohm-GyroBohm model [17]; this enhances numerical stability. 2) Additional axial diffusion is prescribed in the electron temperature channel only: a Gaussian centred the axis with a peak value of 0.1m^2/s and a standard deviation (SD) width of σ = 0.075 in ρ units, which aids numerical stability during W accumulation phases. 3) Since the EM stabilisation correction is ad-hoc, it contains a free parameter; this has not been adjusted to tune predictions (set to 1 in all simulations).

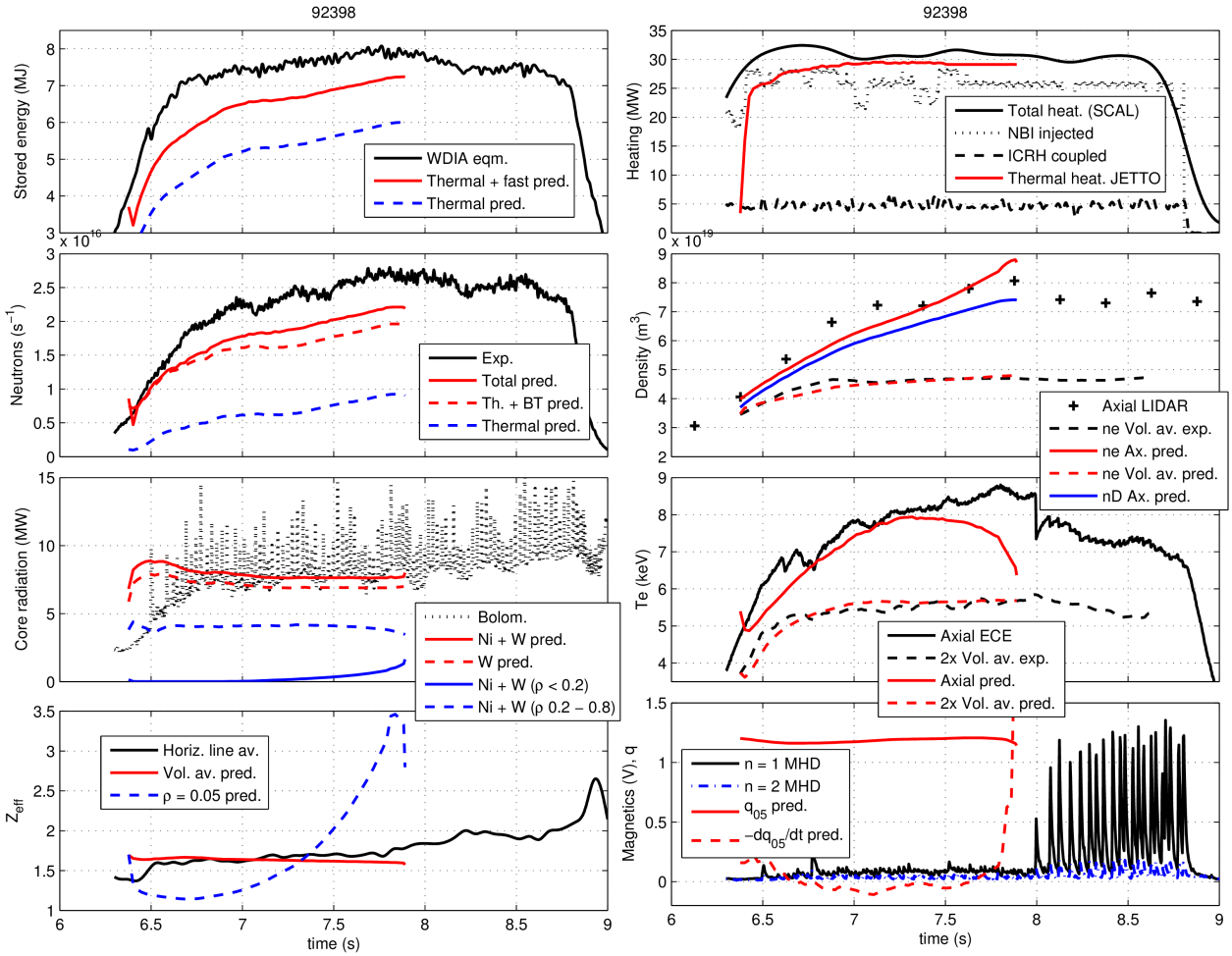

FIG. 2. Evolution of global and axial quantities in JET 92398 compared with predictive multi-channel simulation with JINTRAC. Black curves are experimental data; coloured curves are simulated data. The safety factor at ρ= 0.05 is indicated by q_{05}. Thermal and beam-target neutron rates are predicted self-consistently. NBI-ICRH synergistic enhancement is computed by PION.

3. VALIDATION OF PREDICTIVE CAPABIILITY

To validate the JINTRAC tool and our assumptions above, we simulate the evolution of the second highest performing hybrid pulse (#92398, Bt = 2.8T, Ip = 2.2 MA, NB = 26MW, ICRH = 4.5MW, H_{98} = 1.3 τ_E=0.17s) achieved in JET-ILW to date, from the start of the H-mode, until the accumulation of W on axis 1.6s, 9τ_E later (Figs. 1-3). The density peaking is extremely sensitive to Ti/Te at the pedestal top [18]; larger values of Ti/Te stabilise the ITG mode, Ti/Te changes propagate inwards to the core, and the global stabilisation of the ITG can cause a large increase in density peaking. The value Ti/Te = 1.1, used in the presented simulations gives a density rise which very closely tracks the experiment (Fig. 1). Values of 0.9 < Ti/Te < 1.3 are all within experimental uncertainty. The electron temperature and rotation are also well predicted (Fig. 1). The three impurities are initialised as radially constant concentrations in coronal equilibrium with relative abundances 40:1:0.37 for Be:Ni:W, consistent with spectroscopic measurements, line integrated Z_{eff}, and total radiation. In the experiment, the total core radiation (dominated by W) is broadly constant during the high performance phase. In the simulation the neoclassical pedestal impurity convection is inwards, so there are no impurity losses. No impurity source is required in the simulation to reproduce the measured level of radiation throughout the modelled phases and the total impurity content is constant throughout the simulation. This indicates that the ELM flushing and inter-ELM W transport are in balance in this particular experiment (which maintains a constant ELM frequency with real time control), as also found in an NBI only pulse [3]. The same impurity and pedestal and assumptions are used in the later extrapolated cases.

The simulation reproduces well the global evolution into the high performance phase (Fig. 2), with some under-prediction of the total stored energy and neutron rate, indicating that Ti may be under-predicted. After an initial phase of low field side centrifugal W localisation, neoclassical convection becomes inward and W starts to accumulate on axis from ~7.4s onwards (Fig. 3). Qualitatively, this matches the soft X-ray observations, which show central radiation from 7.7s, although the simulation predicts W increase on axis about 0.3s too early, another sign that the simulation under-predicts central ion temperature peaking and associated impurity screening. Once W starts to accumulate, axial electron temperatures fall, in both simulation and expt. In the simulation, W accum. is sudden and extreme, leading to radiative collapse on axis. This phase of the simulation is *extremely* sensitive, and ultimately becomes numerically unstable when radiation exceeds 2MW in the small volume within ρ < 0.2. In the experiment, the W accum. signals the end of the quiescent highest performance phase, but does not lead to the strong radiative

collapse seen in the simulation. Instead, W accum. is followed within 0.5s by the arrival of (m,n)=(1,1) MHD activity known to regulate W concentration on axis [19]; no attempt is made to model this here. The modelling also reveals that before the W accumulation, the central safety factor is stable above 1, and supported by a large bootstrap current component. However, once the W accumulation is severe, a local loss of bootstrap current causes a drop in the central q; suggesting that W accumulation may be causal in accelerating the arrival of MHD activity. The connection between MHD activity and W accumulation on JET has been widely reported [2,16,20], but not this specific causality.

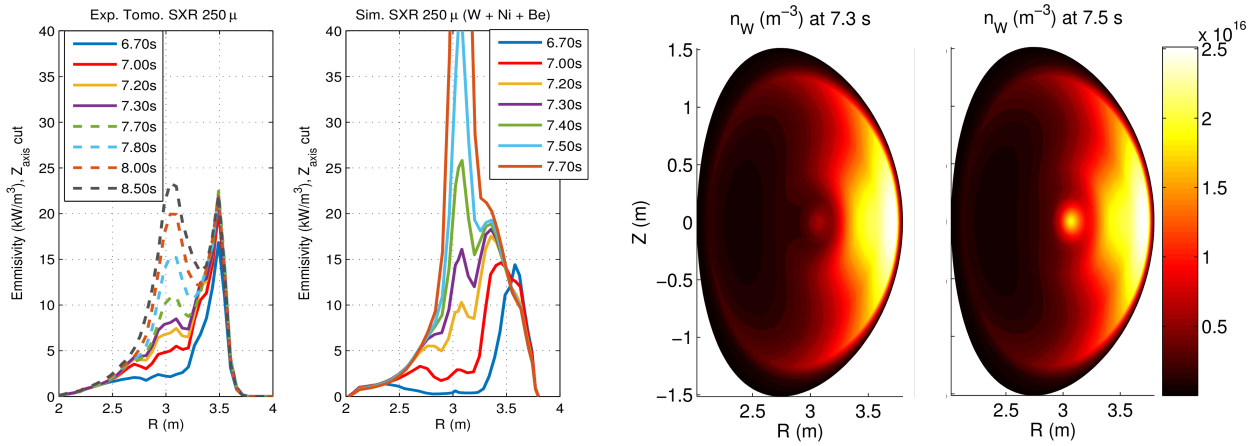

FIG. 3 – (Left) Evolution of soft X-ray tomography for JET pulse 92398 compared to forward modelled SXR emission from W, Ni and Be in predictive simulation. The magnetic axis is at R=3.05m. Before central accumulation, W and Ni are localised on the LFS by rotation. The solid curves are at the same times in sim. and expt., the dashed curves indicate later times in expt. (Right) Predicted W density before and after the start of central accumulation; Ni evolves similarly.

4. OPTIMISATION OF HEATING

We next apply this capability to predict future JET hybrid experiments, to support scenario development to optimise the heating actuators against W accumulation. The next DD campaign on JET plans to increase NBI power to the full rated capacity of 32MW, and to test and optimise different ICRH schemes within the hybrid scenario. In the flux-driven modelling here (unlike above), we prescribe idealised Gaussian ICRH profiles, to allow a systematic study separating the effects of ion/electron heating fraction from power density, and separately show the sensitivities of advanced ICRH models. First, we investigate the impact of heating on W in a power scan (Fig. 4). The increased beam particle deposition associated with increasing NBI power from 26 MW to 32 MW accelerates the density rise, and consequently the W accumulates about 0.7s earlier. The benefit of central ICRH is demonstrated by scanning ICRH power; increasing central RF power drives central turbulence which increases effective D particle diffusivity, delaying the main ion density rise and also increasing turbulent W diffusion. The ion temperature peaking is also increased by ICRH, leading to larger neoclassical temperature screening. Despite these benefits 8MW of localised ICRH power (the maximum foreseen for next JET campaigns) delays the arrival of W on axis by only 1.2s. In terms of the timing of W accumulation, 4MW additional ICRH compensates a 6MW increase in NB power. We also examine the impact of power density by changing the width of the ICRH deposition profiles (Fig. 4). The result shows that the higher power density of a narrow deposition can delay the arrival of W on axis by more than 1s – with localised deposition, the turbulent diffusion extends further towards the axis, and temperature screening is further enhanced by the central Ti peaking resulting from high power density in the neoclassical core. Scans of resonance location demonstrate the same sensitivity to axial power density. These results qualitatively reproduce and explain experimental observations in JET-ILW [21], further demonstrating the predictive capability.

Second, we compare the effects of electron vs ion heating schemes with the same power density for controlling W accumulation (Fig. 5), an optimisation which is not a priori obvious, or known from JET experiments [22,23]. The simulations make a clear prediction, as yet untested for the JET hybrid scenario: ion heating schemes should delay the arrival of W on axis. For localised axial deposition, going from 50% ion heating (typical of H minority) to 80% ion heating (typical of He-3 minority) could delay W accumulation[1] by more than 1s. The ion heating increases effective turbulent diffusion in the region $\rho = 0.2 – 0.4$, reducing density peaking [24]. In the neoclassical core $\rho < 0.2$, the ion temperature peaking and W screening is strongly enhanced by the ion heating. We stress that the benefits of ion heating are *specific to this JET scenario,* with Ti > Te, dominant ITG turbulence for the particle transport, and dominant neoclassical convection for W. Electron heating allows the discharge to tolerate higher levels of W on axis before a radiative collapse, but the ion heating instead delays W accumulation, acting on the bulk profiles to reduce the neoclassical impurity pinch.

[1]A recent experiment in AUG [25] found that ECRH was more beneficial than ICRH (~50:50 ion:electron) in preventing W accumulation. This contrasts with the present predictions, but unlike the JET hybrid, AUG plasmas had weaker i-e coupling and 1,1 MHD activity before W accumulation. The AUG plasmas also have lower Mach number and higher power density, increasing the contribution of turbulent W transport. Future work should compare the turbulent W transport in the JET and AUG conditions.

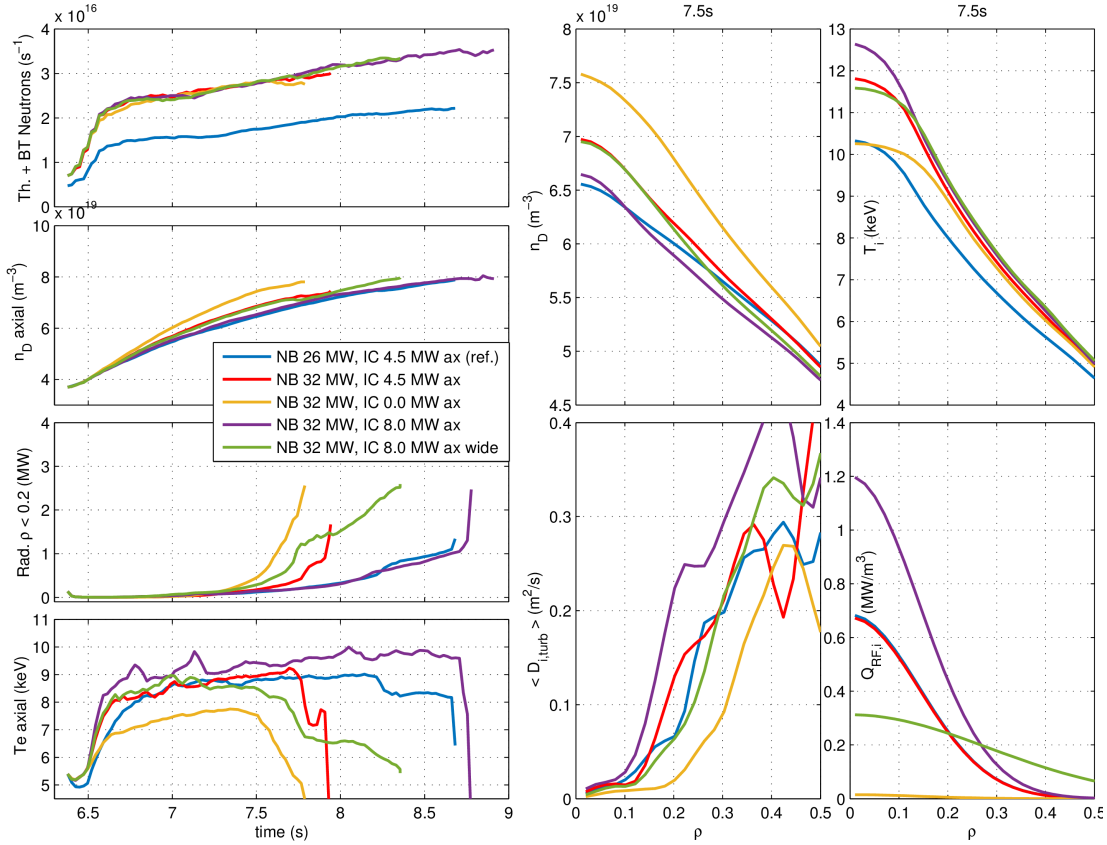

FIG 4 - Impact of NB and IC heating power on timing of W accumulation in predictive simulation. These simulations all use idealised IC heating prescribed as a Gaussian centred on axis with a SD width of σ = 0.14 (ax ,narrow) or σ = 0.28 (ax, wide) in ρ units. The ICRH is 50:50 to ions:electrons, typical of H minority with 2nd harmonic D absorption. The turbulent diffusivity is averaged over 1s preceding the kinetic profile time and is an effective diffusivity (includes turbulent convection). The power densities of the narrow (wide) deposition agree approximately with the TORIC (SCENIC) results in Fig. 6. The peak $Q_{RF,i}$ from PION in the ref. case (Sec. 3) is 0.5 MW/m^2. With increasing RF power, higher T_i is compensated by lower n_D in the neutron yield.

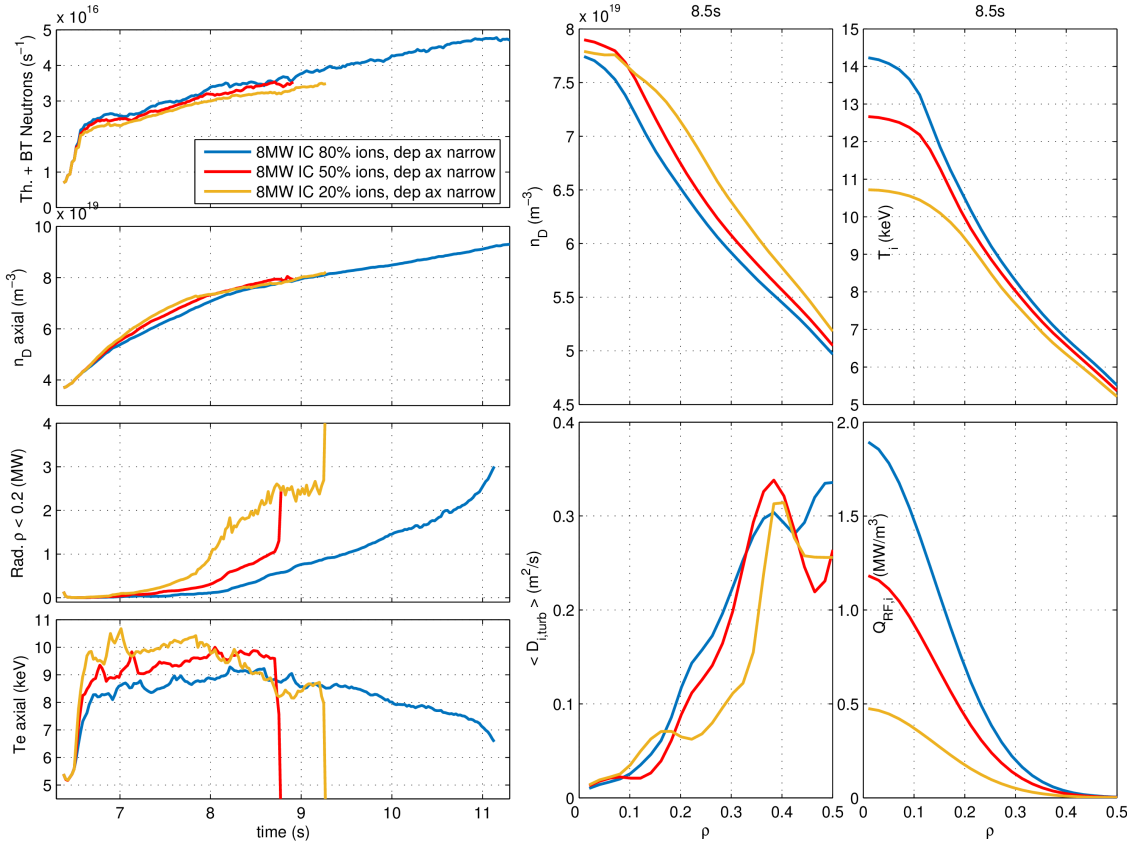

FIG 5 - Impact of ion vs electron IC heating on timing of W accumulation in predictive DD simulation at maximum power. These simulations all have 32MW NB with 8MW idealised IC heating prescribed as a narrow Gaussian centred on axis.

In addition to the strong sensitivity of W accumulation to ICRH power density shown above, previous works have indicated a further benefit of ICRH on W transport, through the influence of fast ion anisotropy (acting to reduce W poloidal asymmetry and neoclassical convection) [4,5,25] and fast ion temperature screening [4,26]. The previous works used TORIC-SSFPQL [27] to compute the resonant minority anisotropy. For this work, a new effort was made to compare the anisotropy predictions of various ICRH models: The SCENIC Monte Carlo package [28,29], features a Fokker-Planck and wave field solution including finite orbit widths (FOW), a self-consistent shaped geometry with fast ion pressure, and an accurate fast ion description. We present a comparison with TORIC for 92398, H minority heating (Fig. 6). The treatment of FOW effects are the significant difference with TORIC-SSFPQL for the presented cases. The results indicate a significantly lower peak power density with FOW effects (anisotropy is correlated with direct absorption power density). The SSFPQL results in Fig. 7 also include magnetic trapping and a preliminary simplified model for FOW, not used in previous W transport studies; both reduce power density and anisotropy. Even with these enhancements to SSFPQL, the two models show significant differences; a detailed analysis of the differences is beyond the scope of this work, but will need to be completed to further refine the modelling of W transport in the presence of ICRH.

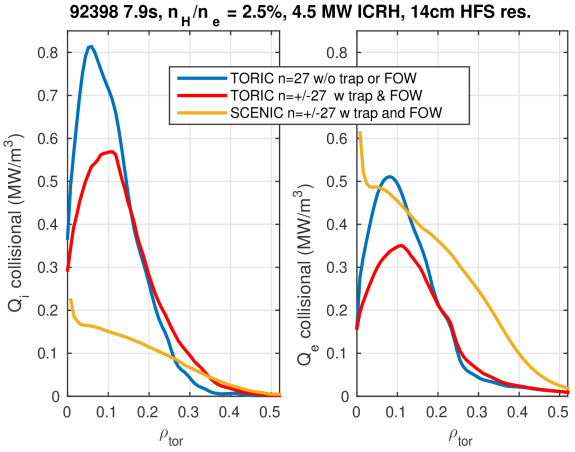

FIG. 6 – Comparision of SCENIC and TORIC-SSFPQL predictions with a HFS resonance as in discharge 92398. The inclusion of trapping and FOW in TORIC both reduce power density and anisotropy. Both codes used a reduced spectrum (n=+/- 27 only). Both wave codes include 2nd harmonic D direct absorbtion, but D beam ions are not included. The 2nd harmonic absorbtion is neglected in the SCENIC Fokker-Planck solver, but is included in SSFPQL.

Compared to previous works [4, 25], we also improved the distribution function used to describe the fast minority population to distinguish between HFS and LFS resonances [30], and used this description to couple the resonant minority distribution from SCENIC to NEO within JINTRAC. The model in [30] nullifies the impact of anisotropy on W for HFS resonances, and reduces it for LFS resonances (for all flux surfaces not tangent to the resonance at the LFS). The net result of the FOW effects and improved minority distribution is to significantly reduce the impact of both fast ions anisotropy and temperature screening on neoclassical W transport, such that their impact on the timing of the W accumulation is negligible (and therefore not included in the results shown above) - the main benefit of ICRH is through the bulk profile influences. This result is consistent with [31], which found a negligible impact of fast ion temperature screening with FOW effects, and [25, 32] which found that the impact of fast ion anisotropy on W asymmetry and transport is likely exaggerated when using TORIC-SSFPQL to provide anisotropy to NEO.

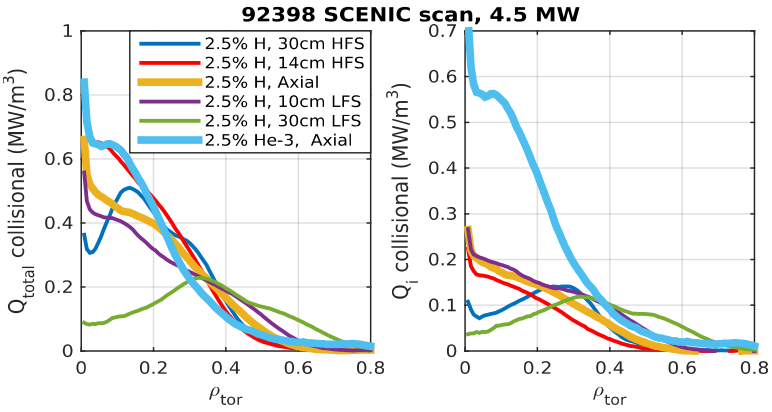

FIG 7 - Scan of resonance locations and H vs He-3 minority heating with SCENIC. In all cases the total coupled power is 4.5 MW and n=+/-27.

Given the sensitivity of the flux-driven predictions, we conduct a scan of resonance location and minority species with SCENIC, to assess the potential for ICRH optimisation (Fig. 7). The results verify the JET-ILW experimental findings that near-axial resonances produce the highest power densities, with limited sensitivity as long as the deposition is within +/- 10cm of the magnetic axis [21,22,26]. The He-3 minority yields a large ion-heating fraction and a slightly narrower collisional power deposition due to increased collisionality and reduced anisotropy. The collisional power densities and deposition width for the He-3 scheme scaled to 8MW are comparable to the narrow idealised heating (80% to ions) used in the multi-channel simulations. The potential for collisional power density optimisation via phasing or fast particle orbit topology remains to be assessed.

5. EXTRAPOLATION TO DT

Finally we apply the predictive tool to examine the impact of isotope on fusion performance and W accumulation. The maximum power DD extrapolations are compared to full tritium plasmas (TT) and DT plasmas (Fig. 8). The DT plasmas are initialised with 50:50 isotope mix, and equal boundary densities ($n_D = n_T = 1.1e19$ m-3). The pedestal feedback controllers give identical transport and total neutral source to each isotope, but neutral penetration is different. The beam sources are configured as they will be in a DT campaign, with one beam box in T and one in D, with the expected energies and energy fractions. The different beam configurations for the isotopes gives deeper

penetration of the D beam ($S_{T,ax}/S_{D,ax}=0.8$ and $S_{T,\rho=0.8}/S_{D,\rho=0.8}=1.3$) but near identical total beam fuelling for each isotope. The fast isotope mixing [33] means that the D:T ratio remains between 53:47 and 50:50 at all locations and times within the simulation. In DT cases, α particle heating is computed following [34]. 8MW ICRH is prescribed, using the narrow Gaussian (80% to ions) found most effective (in Sec. 4) at delaying W accumulation.

The isotope extrapolation (Fig. 8) shows a positive effect on confinement with heavier isotope, due to the inverse ion mass scaling of the ion-electron energy exchange [35]. In all cases, Te is similar due the stiffness of the ETG scale transport. In tritium, the transfer of energy from ions to electrons is less efficient, leading to a larger Ti/Te, known to suppress ITG transport. The resulting enhancement in fusion performance is 31%: at 8.5s (before significant W accumulation), the DD case has a DT equivalent fusion power [36] of 11.3 MW, while the DT case has a predicted fusion power of 14.9 MW. The isotope scaling and predicted fusion power are similar to those presented in [37], albeit with different models and assumptions (in that case no ETG scales were included and the isotope enhancement from ExB shear was stronger). We note that our DT prediction is conservative for the pedestal since we include no pedestal scaling with power or isotope. There are also aspects of isotope transport scaling (in plasmas with Ti = Te) not captured by the present quasilinear models [38]; these could further improve predicted confinement in tritium.

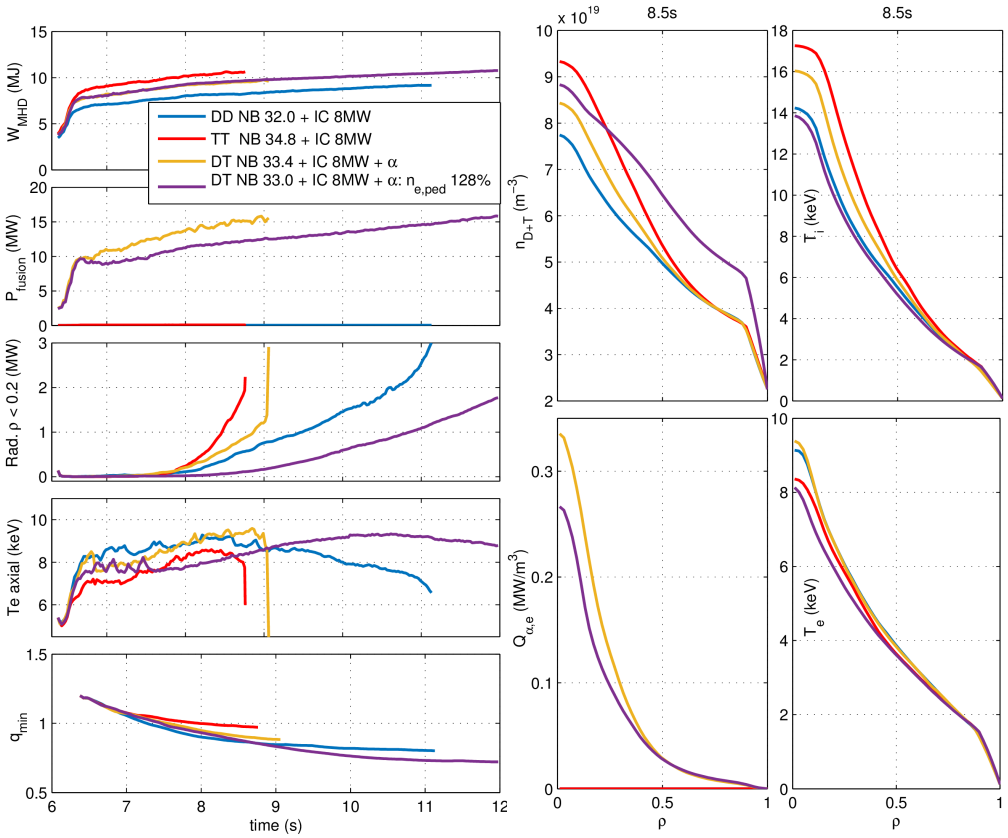

FIG 8 - Impact of isotope and pedestal density on timing of W accumulation and fusion performance in predictive simulation extrapolated to the maximum JET heating power. These simulations all have idealised IC heating prescribed as a narrow Gaussian centred on axis, with 80% delivered to the ions. Minor differences in the maximum NB power are due to different limitations of the beam boxes in different isotopes. The actual performance would be limited by MHD unless the q profile can be further optimised.

Unfortunately, the improved confinement in tritium also leads to additional density peaking, and consequently, earlier W accumulation. One possible solution for a 5s duration hybrid scenario would be to increase density at the pedestal top (either by increased triangularity or plasma current or an isotope dependence [39]), giving less central beam deposition and a slower timescale for density peaking. In the simulated case, an increase in the pedestal top density of 28% delays W accumulation by 2s, with a 20% loss in fusion performance at 8.5s. However, the current diffusion in the extended simulated pulse indicates $q_{min} < 1$, well before significant W accumulation. A fully integrated solution for the scenario will therefore require tailoring of the q-profile during ramp-up, or a strategy which tolerates 1,1 MHD but avoids tearing modes. The present simulations (with no MHD model) continue to predict increasing density, stored energy and fusion performance after $q_{min} < 1$. Likely this evolution is determined by the resistive timescale, in any case, the actual performance would be limited by MHD unless the q profile can be further optimised; future modelling will investigate long duration performance with an MHD constrained q-profile.

Increasing power and isotope mass are also expected to increase the source of W from divertor sputtering. To test the impact of this on the scenario, we have performed simulations with a 50% increase in the total W content, giving 23MW radiation (not shown). As with the small impact of α heating (electron heat source), the scenario evolution is insensitive to this increase in the electron heat sink, due to the stiffness of the electron heat channel. Ref [3], which excluded ETG scales, reported increased performance with increased radiation due to increasing Ti/Te; in the present work this effect is now absent due to the inclusion of ETG scales. We have also compared DT simulations with and

without α heating and found it makes only minor differences to scenario performance or the timing of the W accumulation; since the ETG scales give very stiff electron transport, stored energy is insensitive to electron heating: The inclusion of α heating increases axial electron temperature by ~5%, and drives more turbulence, which slightly delays the density peaking and W accumulation by ~0.25s. Paradoxically, the 2.5MW alpha heating leads to ~4% lower fusion power before W accumulation, due to the delayed density rise (no effect on Ti).

6. SUMMARY and DISCUSSION

This work demonstrates the integration of multiple first-principle based models into a powerful multi-channel predictive tool for the core plasma, which can reproduce observed W accumulation and ICRH mitigation in JET, and is able to guide JET scenario development. The modelling capability is applied to investigate the optimal ICRH scheme to resist W accumulation in the hybrid scenario, scanning power density and resonant minority (H and He-3), to help JET reach its objective of high performance in steady conditions (5s). High power density located near the axis, preferably with dominant ion heating, is predicted to be most effective in delaying the central accumulation of W, in JET hybrid conditions. Supporting high-fidelity ICRH modelling (including the effects of finite orbit widths) finds that these requirements can be met by axial He-3 minority heating, which will deliver both higher power density and greater ion heating compared to H minority schemes. The modelled system contains multiple non-linearities, and the W accumulation phase is extremely sensitive to heating power density. As such, the present predictions are qualitative, and further cross-code validation effort is needed to improve confidence particularly in the ICRH modelling. The inclusion of finite orbit width effects within the ICRH models appears to be an important element, which reduces the impact of fast ions on W transport, and spreads the power deposition.

The modelling capability has also been used to predict scenario and W evolution in planned TT and DT plasmas, and predicts improved confinement with heavier isotope, due to decreased ion-electron coupling, increased Ti/Te and stabilisation of the ITG mode. Extrapolations to full power (40MW) DT plasmas predict 15MW of fusion power with conservative pedestal assumptions. Unfortunately, the improved confinement comes with greater density peaking and a tendency for earlier W accumulation, which will make achievement of a stationary hybrid scenario a challenge. Increasing the pedestal density presents one solution; less central beam deposition delays density peaking and W accumulation, at some cost in fusion power. Future modelling and experiments will seek an optimisation between plasma current, pedestal density, q profile evolution and performance to build a stationary high performance hybrid plasma. It remains to be demonstrated if stationarity can be achieved in MHD-free conditions, or if benign 1,1 MHD activity can be tolerated. The predictions made here for isotope scaling and W accumulation are specific to plasmas with Ti > Te, and depend on the inclusion of ETG transport within a quasilinear transport model, which remains to be verified by non-linear multi-scale gyrokinetics in these conditions. These predictions are made in advance of planned experiments and will be tested as JET operates with higher power and tritium isotope in the coming campaigns.

ACKNOWLEDGEMENTS and REFERENCES

This work has been carried out within the framework of the EUROfusion Consortium and has received funding from the Euratom research and training programme 2014-2018 under grant agreement No 633053. The views and opinions expressed herein do not necessarily reflect those of the European Commission. F.J. Casson wishes to thank all those who have contributed to the JINTRAC codes over many years, and C. M. Roach and J. Garcia for helpful discussions.

[1] Joffrin, E. OV/1-3, IAEA-CN-258 FEC (2018); **[2]** Angioni, C. et al. Tungsten transport in JET H-mode plasmas in hybrid scenario... NF 54, 83028 (2014); Angioni, C. et al. The impact of poloidal asymmetries on tungsten transport in JET... PoP 22, 55902 (2015); Romanelli, M. & Ottaviani, M., Effects of density asymmetries on heavy impurity transport... PPCF 40, 1767 (1998); **[3]** Breton, S. et al. First principle integrated modeling of multi-channel transport including Tungsten in JET. NF 58, 96003 (2018); **[4]** Casson, F. J. et al., '...heavy impurity transport and ... modelling of tungsten in JET and AUG', PPCF, 57 (2015),14031; **[5]** Angioni, C. & Helander, P., Neoclassical transport of heavy impurities with poloidally asymmetric density. PPCF 56, 124001 (2014); **[6]** Belli, E. A. and Candy, J., a) PPCF, 50 (2008), 95010 ; b) PPCF, 51, (2009) 75018; c) PPCF, 54 (2012), 15015; **[7]** Bourdelle, C. et al., Core turbulent transport in tokamak plasmas… with QuaLiKiz, PPCF, 58 (2016), 14036; **[8]** Citrin, J. et al., Tractable flux-driven temperature, density, and rotation with... QuaLiKiz, PPCF, 59, 124005 (2017); **[9]** Cenacchi, G. and Taroni, A., JETTO: A Free-Boundary Plasma Transport Code, Internal report JET-IR(88)03, (1988); **[10]** Romanelli, M. et al., JINTRAC: A system of codes for Integrated Simulation of Tokamak Scenarios, Plasma and Fusion research, 9 (2014), 3403023; **[11]** Ho., A.et al., Turbulent transport model validation against a JET plasma via integrated modelling... NF submitted (2018); **[12]** Citrin, J. et al. Electromagnetic stabilization of tokamak microturbulence in a high- β regime. PPCF 57, 14032 (2015); **[13]** Challis, C.D. et al., NF 29 (1989) 563; **[14]** Eriksson, L-G. et al NF 33 (1993) 1037; **[15]** Tomar, S. JCP 40 (1981) 104; **[16]** Pütterich, T. et al. PPCF 55, (2013) 124036; EX–P3.15 IAEA-CN-197 FEC (2012); **[17]** Erba, M et al, PPCF 39 (1997) 261; **[18]** Maggi, C. F. et al. Isotope effects on L-H threshold and confinement in tokamak plasmas. PPCF 60**,** 14045 (2018). Linder O, et al. Flux-driven integrated modelling ... in AUG, NF, (2018) submitted; **[19]** Sertoli, M. et al. PPCF 53, 035024 (2011); Sertoli, M. et al. PPCF 57, 075004 (2015); **[20]** Hender, T. C. et al. The role of MHD in causing impurity peaking in JET.... NF 56, 66002 (2016); **[21]** Lerche, E. et al. Optimization of ICRH for core impurity control in JET-ILW. NF 56, 36022 (2016); **[22]** Eester, D. V. et al. Recent H majority inverted radio frequency heating scheme experiments in JET-ILW. EPJ Web Conf. 157, 3061 (2017); **[23]** Puiatti, M. E. et al. Analysis of metallic impurity density profiles in ...JET. PoP 13, 42501 (2006); **[24]** Angioni, C. et al. Off-diagonal particle and toroidal momentum transport.... NF 52, 114003 (2012); **[25]** Angioni, C. et al. A comparison of the impact of central ECRH and central ICRH on W behaviour in AUG. NF 57, 56015 (2017); **[26]** Goniche, M. et al. ICRH for W control in ... JET scenarios. PPCF 59, 55001 (2017); **[27]** Brambilla, M. & Bilato, R. ...numerical simulations of ICH of non-Maxwellian plasmas. NF 49, 85004 (2009); **[28]** M. Jucker et al. , 'Integrated modeling for ICRH in toroidal systems', CPC., 182 (2011), 912; **[29]** W. A. Cooper et al., Anisotropic pressure bi-Maxwellian distribution.., NF, 46 (2006); **[30]** R. Bilato et al., impact of ICR location on poloidal asymmetries of impurity density..., NF, 57 (2017), 56020; **[31]** Gallart, D. et al. Modelling of JET hybrid plasmas with … combined ICRF and NBI heating. NF 58, 106037 (2018); **[32]** M. Sertoli et al, Effects of ICRH resonance on ... W density..., EPS 2018 O4.103; **[33]** Bourdelle, C. et al. Fast H isotope mixing... NF 58**,** 76028 (2018); **[34]** Kamelander, G. & Sigmar, D. J. Phys. Scr. 45, 147 (1992); **[35]** Schneider, P. A. et al. Explaining the isotope effect with collisional electron-ion energy exchange. NF 57**,** 66003 (2017); **[36]** Garcia, J. TH/3-1, IAEA-CN-258 FEC (2018); **[37]** Garcia, J. et al. Challenges in extrapolation from DD to DT... PPCF 59**,** 14023 (2017); **[38]** Weisen, H. EX/P1-4, IAEA-CN-258 FEC (2018); **[39]** Maggi, C. F. et al. Isotope effects on L-H threshold and confinement.... PPCF 60**,** 14045 (2018).